Available online at www.sciencedirect.com

ScienceDirect

Advances in Space Research 68 (2021) 1263–1280

ADVANCES IN SPACE RESEARCH (a COSPAR publication)

www.elsevier.com/locate/asr

Review

Review of recent GNSS modelling improvements based on CODEs Repro3 contribution

Rolf Dach [a,*], Inga Selmke [b], Arturo Villiger [a], Daniel Arnold [a], Lars Prange [a], Stefan Schaer [a,c], Dmitry Sidorov [a,d], Pascal Stebler [a], Adrian Jäggi [a], Urs Hugentobler [b]

[a] Astronomical Institute, University of Bern, Sidlerstrasse 5, CH-3012 Bern, Switzerland
[b] Institute for Astronomical and Physical Geodesy, Technical University of Munich, Arcisstraße 21, DE-80333 München, Germany
[c] Swiss Federal Office of Topographie, swisstopo, Seftigenstrasse 264, CH-3084 Wabern, Switzerland
[d] Now with Leica Geosystems, Heinrich-Wild-Strasse, CH-9435 Heerbrugg, Switzerland

Received 15 February 2021; received in revised form 24 April 2021; accepted 27 April 2021
Available online 8 May 2021

Abstract

The Center for Orbit Determination in Europe (CODE) is contributing to the most recent reprocessing effort of the International GNSS Service (IGS) with a triple-system solution including GPS (since 1994), GLONASS (since 2002) and Galileo (since 2013). Several model improvements with respect to the operational processing scheme have been implemented and applied for the reprocessing effort: The first group of improvements is related to the update of IERS-related models (mean pole and high-frequency pole models). The second group is related to the inclusion of Galileo with calibrated receiver and satellite antennas. The consistency of the scale for the ground station coordinates was verified based on the estimation of GNSS-specific coordinate biases. It turned out that currently widely used GPS-based receiver antenna calibrations do compensate (just by chance) a discrepancy in the scale when using the pre-launch satellite antenna calibrations for Galileo.

Furthermore and third, a long-arc solution over three days is introduced where in particular empirical velocity changes are rescheduled with respect to the operational processing chain at CODE. Instead of simply estimating them every 12 h they are now setup at orbit midnight. This rescheduling reduces the size of orbit misclosures by 10% for GPS and 15% for Galileo; no improvement for GLONASS was observed because there the orbit misclosures are dominated by other effects. Another feature applied for the first time in this reprocessing series is to downweight the observations of a number of GPS satellites with a reduced stability in the attitude control around the year 2000. This change in the analysis strategy reduces the noise level of GNSS-derived products, e.g., of the Earth rotation series.

Even if the article is focusing on the reprocessing series as provided by the CODE analysis center many of the conclusions may also be applied to other GNSS series in future.

Keywords: CODE reprocessing; GNSS reprocessing; GNSS orbit modeling; Weighting of historic GPS data

Contents

* Corresponding author.
E-mail address: rolf.dach@aiub.unibe.ch (R. Dach).

https://doi.org/10.1016/j.asr.2021.04.046
0273-1177/

1. Introduction

In preparation of the next release of the International Terrestrial Reference Frame ITRF 2020), the International GNSS Service (IGS, Johnston et al., 2017) has asked for contributions to its 3rd reprocessing campaign (so called repro3). The most recent developments and experience from the operational processing of the Global Navigation Satellite System (GNSS) observations were consistently applied to the dataset of more than 25 years. With this initiative the best possible IGS contribution to the ITRF2020 shall be guaranteed.

The Center for Orbit Determination in Europe (CODE) acts as a global Analysis Center (AC) of the IGS. It is a joint venture between the Astronomical Institute, University of Bern (AIUB), Bern; the Federal Office of Topography swisstopo, Wabern, both Switzerland; the Federal Agency of Cartography and Geodesy (BKG), Frankfurt a. M.; and the Institute for Astronomical and Physical Geodesy, Technical University of Munich (IAPG/TUM), Munich, both Germany. CODE supported already the previous reprocessing campaigns of the IGS (Steigenberger et al., 2011; Steigenberger et al., 2014) and reprocessing activities related to other projects (e.g., Fritsche et al., 2014; Sušnik et al., 2020).

The operational processing strategies are under constant evaluation in order to identify potential modelling deficiencies and to improve the solutions. These developments are well documented in the annual reports to the IGS (e.g., Dach et al., 2020, as the most recent one). Several detected modelling shortcomings have been addressed to obtain the best possible reprocessing products for CODE's reprocessing contribution. These modelling updates can be realized either by configuration changes or may require additional developments in the underlying software package, the Bernese GNSS Software (Dach et al., 2015). Some of these modeling extensions were related to the IERS conventions (Petit and Luzum, 2010, where IERS stands for International Earth Rotation and Reference Frame Service), others followed agreements between the IGS ACs, and a third group was compiled by most recent progress at CODE when analyzing operational and other recent reprocessing product series.

This paper describes the latest improvements for the satellite modelling at CODE which have been implemented for the IGS repro3 effort. We will assess in the various steps of the transition from the operational CODE final solution series to the analysis strategy for reprocessing the GNSS data as it is implemented at CODE for the IGS repro3 effort. This procedure allows us to assess the influence of model changes and improvements on the solution series in detail.

The paper starts with a description of selected key aspects of the CODE reprocessing solution. The applied model changes and improvements are grouped and introduced step by step. At each step, the influence on the derived GNSS results are discussed. The first step consist of replacing the conventional IERS models by the models agreed upon by the IGS ACs (Section 3). The next step describes the inclusion of Galileo as the third GNSS besides GPS and GLONASS (Section 4). In this context the antenna modeling is of particular interest. Section 5 describes the strategy to derive long-arc solutions over three days and focuses on handling of orbit modeling deficiencies during satellite eclipse. Last but not least, in the early years of the reprocessed time span some of the GPS satellites show a non-nominal behavior requiring downweighting of observations to specific satellites in order to not degrade the GNSS-derived products (see Section 6). A summary and conclusions are provided in Section 7.

2. Description and basic characteristics of the CODE repro3 solution

The CODE repro3 solution provides a consistent series of GNSS-derived parameters starting from the beginning of the IGS operations in January 1994 as a GPS-only solution. As already in earlier reprocessing solutions, the early years of the International GLONASS Experiment (IGEX, Willis et al., 2000) are not considered because of the instability of the satellite constellation. GLONASS is included in the solution since year 2002. At that time less than ten GLONASS satellites were active; the constellation was completed in December 2011 by typically up to two triple-launches per year. Within the last years from time to time one or two slots in the constellation were not occupied by active satellites. Initially, only few stations (mainly located in Europe) supported tracking of GLONASS satellites. This number increased continuously with time. Since

about 2009 a global tracking of the GLONASS satellites is possible.

A similar development took place for the Galileo constellation. The first four satellites are included in the reprocessing solution starting with year 2013; the full constellation was achieved with the activation of the 24th satellite in early 2019. In the frame of the MGEX pilot project (Multi-GNSS extension, Montenbruck et al., 2017) of the IGS the tracking capability of many IGS sites was quickly extended. Already during the year 2015 a global coverage of Galileo tracking stations was achieved. The inclusion of Galileo is new in reference frame relevant product lines, e.g., the legacy final solutions – even though CODE provides Galileo orbits and satellite clock corrections as the first AC of the IGS in their legacy rapid and ultra-rapid solution since September 2019 (Dach et al., 2020).

Figs. 1 and 2 show the development of the number of satellites included in the CODE reprocessing solution from each of the three systems as well as the number of stations providing the related observations illustrating the above statements.

The station selection was based on the priority list agreed upon between the ACs (see http://acc.igs.org/repro3/repro3_station_priority_list_060819.pdf; accessed in September 2019), considering aspects like collocation sites with other space-geodetic techniques, long history of time series. In addition, the availability and the content of observation files was evaluated prior to the definitive station selection. A global coverage for all considered GNSS was targeted as early as possible in the time line of the product generation. Another important aspect was to include

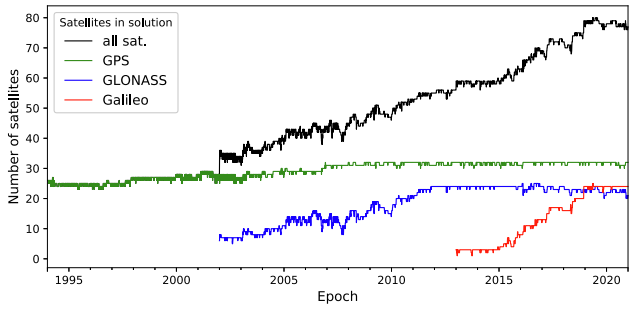

Fig. 1. Number of satellites in the reprocessing solution.

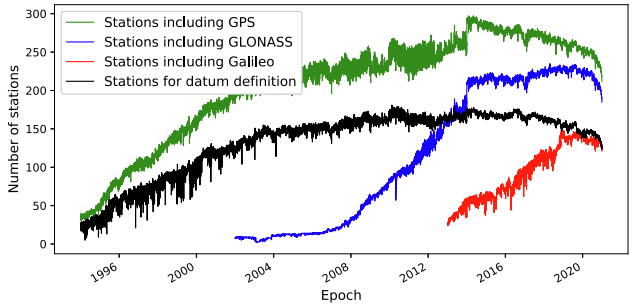

Fig. 2. Number of stations in the reprocessing solution.

only stations equipped with antennas for which a multi-GNSS receiver antenna calibration is available (observations were not considered in the repro3 processing when no calibrations were available for the related GNSS and just the values from GPS are applied for other GNSS; apart from the dedicated experiment in Section 4). Apart from a few stations which were already active in the 1990s, stations were also left out when the calibration with the correct radome was not available (according to the practice within the IGS the calibration from the same antenna, but without a radome should be used instead). Due to these restrictive selection criteria regarding the antenna calibration, the best possible consistency of the obtained coordinates with the antenna reference point shall be achieved. An upper limit of 300 stations per day was applied in order to optimize the processing time as well as the memory and harddisk consumption to the available computer resources.

The detailed modeling is described in the "IGS Analysis Strategy Summary" (provided at ftp://ftp.aiub.unibe.ch/REPRO_2020/CODE_REPRO_2020.ACN); an overview of some key parameters is provided in Table 1. The general processing chain was organized as follows:

1. After pre-processing the observations starting from RINEX observation files, a normal equation (NEQ) containing all relevant parameters was generated for each day based on phase-only double-difference observations with resolved initial carrier phase ambiguities.
2. An initial solution for each day was computed solving for station coordinates, troposphere parameters, orbital parameters, Earth rotation parameters (ERPs), and remaining phase ambiguity parameters that have not been resolved to their integer values.
3. Consistency of satellite orbits and station coordinates for consecutive days has been checked.
4. The NEQs from three consecutive days (from step 1) were combined to a three-day solution as described in Section 5 providing continuous estimates for station coordinates, troposphere parameters, orbit parameters, and ERPs over 72 h.
5. The solution for the geometry parameters was introduced in a zero-difference combined code- and phase-measurement analysis in order to obtain epoch-wise receiver and satellite clock corrections with a sampling of 300 s together with the relevant code- and phase-biases (following the principle of observable-specific signal biases (OSB), Villiger et al., 2019; Schaer et al., 2020).
6. In two further steps these clock corrections were densified by a phase-based interpolation (Bock et al., 2009) from 300 s to 30 s and 5 s, respectively.

In this paper the focus is set on the model updates related to the double-difference solution (steps 1–4); the remaining two steps are only listed for completeness. The

Table 1
Selected modeling aspects for the GNSS processing of the CODE contribution to the IGS repro3.

Observation selection	Phase measurements[a] from GPS since 1994; from GLONASS since 2002; from Galileo since 2013 with baseline-wise resolved ambiguities: • Melbourne-Wübbena based widelane/narrowlane method (<6000 km for GPS and Galileo) • Quasi-ionosphere free (QIF) approach for ambiguities not resolved in previous step (<2000 km for GPS and Galileo; GLONASS, same frequencies) • Phase-based widelane/narrowlane method (<200 km for GPS, Galileo, and GLONASS without restrictions) • Direct L1/L2 method (<20 km for GPS, Galileo, and for GLONASS without restrictions) (detailed description of these algorithms in Dach et al., 2015) Please note that the observations from all GNSS are introduced with the same weight and do fully contribute to all estimated (and relevant) parameters.
A priori SRP orbit model	None for GPS and GLONASS; Galileo satellite properties from GSA (2017) implemented
Albedo modeling	Modeled according to Rodriguez-Solano et al. (2012)
Satellite orbit parameters	Initial conditions and empirical orbit parameters according to the ECOM-decomposition with constant and twice-per-revolution in D; constant in Y; as well as constant and once-per-revolution terms in B (Arnold et al., 2015); stochastic pulses (Beutler et al., 1994) in along-track, radial, and out-of-plane with constraints of $10^{-5}, 10^{-6}, 10^{-8}$ m/s
Orbital arc length	Three-day solutions, see Section 5
Satellite attitude modelling	GPS: Kouba (2009); GLONASS: Dilssner et al. (2011); Galileo: GSA (2017)
Datum definition	Minimum constraint solution using a verified list of reference frame stations in IGSR3 frame[b]
Antenna corrections	IGSR3 antenna correction model (including GNSS-specific receiver antenna corrections)[c]
Troposphere modeling	VMF1 (Böhm and Schuh, 2004) with 2-hourly resolution of station-specific troposphere parameters, gradients (Chen and Herring, 1997) with daily resolution
Ionosphere modeling	Ionosphere-free linear combination and higher order ionosphere corrections (2nd and 3rd orders) as well as ray-bending (Brunner and Gu, 1991; Bassiri and Hajj, 1993)
Elevation mask	3° with elevation-dependent weighting ($\sin^2(e)$)
Sampling rate	30 s for pre-processing and ambiguity resolution; 180 s for the final solution

[a] Pseudorange observations are only used for the ambiguity resolution based on Melbourne-Wübbena linear combination and in the clock/bias product generation step that is not discussed in this paper.
[b] ftp://igs-rf.ign.fr/pub/IGSR3/IGSR3_2077.snx (accessed January 2020)
[c] ftp://ftp.aiub.unibe.ch/users/villiger/igsR3_2077.atx (accessed January 2020)

Table 2
Parameters included in the one- and three-day solutions for the GNSS processing of the CODE contribution to the IGS repro3.

Parameter	1-day	3-day	Remark on the 3-day solution
Station coordinates	3 per station	3 per station	continuous over 72 h[a]
Vertical troposphere parameters	13 per station	37 per station	continuity due to piece-wise linear representation
Troposphere gradient parameters	2 × 2 per station	4 × 2 per station	continuity due to piece-wise linear representation
GNSS-translation biases	removed[b]	removed[b]	only estimated for special solution, see Section 4
Earth rotation parameters	5 parameters[c]	11 parameters[c]	continuity due to piece-wise linear representation[a]; one UT parameter is fixed to the related values in the IERSC04(14)-series (Bizouard et al., 2019)
Geocenter coordinates	removed[b]	removed[b]	3 parameters included in the SINEX result file
Orbital elements	6 per satellite	6 per satellite	one orbit arc over 72 h
Dynamical orbit parameters	7 per satellite	7 per satellite	one orbit arc over 72 h
Stochastic orbit parameters	≈ 6 per satellite	≈ 18 per satellite	at orbit midnight epoch for 3 components, see Section 5
	removed from the NEQ if they are closer than 6 h to end of the orbital arc		
Satellite antenna offset parameters	removed[b]	removed[b]	3 parameters per satellite for the SINEX result file
Satellite antenna phase patterns	removed[b]	removed[b]	intended for further investigations

[a] Description of the technical details are provided in Section 5; special handling in Section 3
[b] The related parameters are removed from the NEQ and the right hand side vector, which corresponds to an infinitely strong constraint
[c] 2/4 sets × 3 components - 1 UT-value = 5/11 parameters for 1-/3-day solution, respectively.

parameters estimated in these steps are summarized in Table 2.

A minimum constraint solution is performed for each day. Station coordinates are estimated using no-net translation and no-net rotation conditions with respect to the reference frame (IGSR3, the IGS-specific realization of the ITRF2014 adapted for the IGS repro3 campaign). The estimated coordinates are compared with the coordinates in the given reference frame. Those stations with deviations greater than 1 cm in the horizontal and 3 cm in the vertical components are not used for the datum definition. Typically, only 1 to 2 stations are excluded per day (in maximum 5 stations out of more than 100 reference frame sites). Finally, only the verified list of stations was

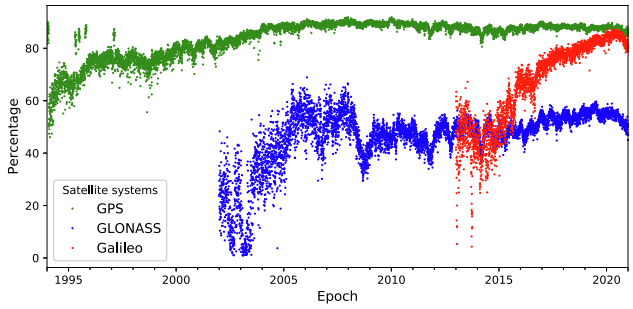

Fig. 3. Percentage of resolved ambiguities in the CODE repro3 solution.

used for the datum definition. Their number per day is shown as the black curve in Fig. 2.

With the increasing number of Galileo tracking sites more and more equipment changes might have introduced inconsistencies with the reference frame coordinates because of the uncertainty of receiver antenna calibrations. In some cases also new stations have been introduced in order to improve the Galileo tracking where most of them don't have coordinates in the IGS R3 coordinate set. As a consequence the number of reference frame sites decreases starting from 2016 onward from 150 to 120 (as shown in Fig. 2) what still seems to be sufficient for a reliable datum definition.

As a quality measure of GNSS solutions, Fig. 3 shows the percentage of resolved initial carrier phase ambiguities. According to the procedure described in Table 1, the applied strategies depend on the length of the baselines implying that in the case of a sparse network the resolution rate cannot be very high (see, e.g., the blue and red curves for GLONASS and Galileo, respectively). The limited resolution rate for GLONASS until the end of the series can be explained by the condition that only ambiguities for the same frequency are allowed to be resolved for baselines longer than 200 km. On the other hand, nearly all GLONASS intra-frequency ambiguities are successfully resolved. It is also interesting that for comparable baseline lengths more ambiguities for Galileo observations are successfully resolved with the Melbourne-Wübbena approach than for GPS. After applying the QIF strategy to resolve also the remaining ambiguities the resolution rate for GPS and Galileo is in the same order of magnitude. As the Melbourne-Wübbena ambiguity resolution uses the pseudorange measurements as well, this characteristic can be viewed as an indication for the high quality of the Galileo code observations. The short periods in the 1990s with a higher resolution rate for GPS are related to intervals when the anti-spoofing function was temporary switched off.

3. Impact of the IERS-related modelling changes

The IERS conventional and background models were updated in the following respects:

- mean pole model (Petit and Luzum, 2010, v 1.2.0),
- high-frequency pole model (Desai and Sibois, 2016), and
- ocean tidal loading corrections for station displacement and gravitational effect on satellite orbits is now based on FES2014b (Carrere et al., 2016).

The first of the three updated models can be interpreted as a datum parameter for the ERP impacting not only the estimated ERPs but also for asking for a related datum in the gravity field representation (see King and Watson, 2014). In particular the oblateness of the Earth introduces a twice-per-revolution effect on the orbits resulting in an effect in the subdaily domain. For the last two model changes the impact in the subdaily frequency domain of the GNSS solutions is obvious.

When comparing the displacements of the summed-up tidal components for the crustal deformations of FES2004 (Lyard et al., 2006) and FES2014b for the stations included in the CODE reprocessing, no systematic effects can be detected (see Fig. 4). There is a limited number of stations showing significant differences between these two models: only 4 stations exceed 2 mm limits in the horizontal and 2 stations show differences of more than 2 cm in the vertical components (17 stations show more than 1 cm). These sites are located at the South coast of Alaska and along the English Channel. As the changes in the ocean tidal loading deformations for the GNSS ground station network are very small or regionally restricted, the impact on a global GNSS solution is limited. The influence of the gravitational effect on the GNSS satellites is so small

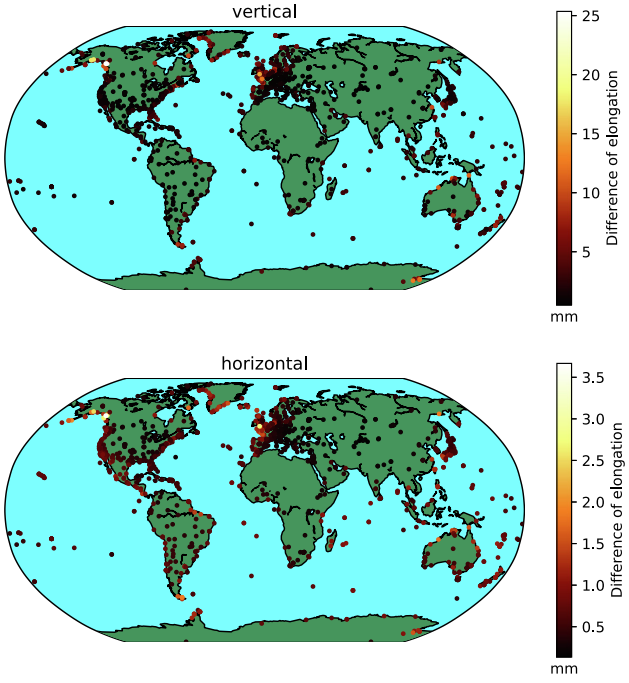

Fig. 4. Maximum differences between the ocean tidal loading displacements based on FES2004 and FES2014b, respectively; summed effect over all tidal components typically used in the GNSS data analysis.

that the model update changes the orbits on the one millimeter level at maximum.

A larger effect instead can be expected from the replacement of the high-frequency pole model. As the ERPs are set up as parameters with daily resolution (with offset and rate), aliasing periods can be expected in a spectrum of ERP estimates. Because such aliasing periods do not only depend on the sampling of the ERPs but also on the revolution period (or more precisely on the geometry repetition period between the satellite and the ground stations, Penna et al., 2007; Stewart et al., 2005), different effects for each of the three considered GNSS will result. Abraha et al. (2018) have demonstrated the different propagation characteristics of various tidal frequencies into GPS and GLONASS series, respectively.

For these reasons three consistent series of ERPs for each of the GNSS have been derived, following the approach introduced by Scaramuzza et al. (2018). This means that one multi-GNSS solution is computed, where separate ERPs are set up independently for each GNSS. The discontinuities of the ERP values at the midnight epoch are computed for day i and i+1 from the polar motion offset x and rate $\dot{x}$:

$$x_i(24\text{ h}) = x_i(12\text{ h}) + \frac{\dot{x}_i}{2} \quad (1)$$

$$x_{i+1}(0\text{ h}) = x_{i+1}(12\text{ h}) - \frac{\dot{x}_{i+1}}{2} \quad (2)$$

Since the polar motion components $x_i(24\text{ h})$ and $x_{i+1}(0\text{ h})$ refer to the same epoch, the spectral analysis of their difference provides according to Kouba (2003) an insight in the high-frequency pole model (of course overlayed by the revolution period of the satellite orbits as described above). For this purpose, daily independent ERP values are needed at the midnight epoch. Using the polar motion series from our one-day solution we obtained a noisy spectrum with peaks at 200 to even 500 μas whereas the peaks are ten times smaller when comparing the offset values at noon to a reference series (like, e.g., IERS C04(14)-series, Bizouard et al., 2019, where the rates from the reference can be used for interpolation). This demonstrates that the polar motion rates are quite uncertain when computing only one-day solutions (as already reported in Lutz et al., 2016). With longer orbit arcs the stablity of the estimated polar motion rates do improve.

For these reasons, the procedure to generate the three-day long-arc solution (described in Section 5) was modified by not applying the constraints on the piece-wise linear ERP parameters at midnight. The results from ERP discontinuities as obtained from the GNSS-specific solutions are shown in Figs. 5b–d together with a conventional series of ERPs where all GNSS are contributing to one and the same ERP series (Fig. 5a). As already pointed out by Scaramuzza et al. (2018), GPS has better capabilities to compute ERP series than other systems like GLONASS and Galileo because GPS is based on six instead of three orbital planes. This is clearly visible in the higher general noise in the spectra in Figs. 5c and d compared to Fig. 5b.

For GLONASS a dedicated high noise is visible in the range of 7 to 8 days period. The constellation repeats after 8 sidereal days (and 17 revolutions of the satellites). That this period does not appear that clear is related to the fact that several GLONASS satellites have been inactive for a longer interval during this three years time span. The related period of 10 days in case of Galileo is not pronounced because the constellation was rather incomplete during a long time where these strectra are computed from.

The most prominent periods in the combined solution (Fig. 5a) are at 14.8 days (mainly in the Y-component) and 14.2 days (in both components). The magnitude of the first one is reduced by updating the models, whereas the magnitude of the latter one is amplified. Looking through the series of the individual GNSS (Figs. 5b–d) the same behavior for these periods can be observed but to a different extent. This consistent behavior indicates that the peaks at these periods are likely really related to the high-frequency pole model.

For many amplitudes at other periods, an improvement or degradation of the series for the individual GNSS can be found. In summary, there are more cases with a moderate improvement than with a degradation. These effects are not detectable to the same extent in the combined series, which is expected, because the orbit characteristics of different satellite systems are overlayed and the magnitude of GNSS-specific effects is reduced.

Numerous tidal constituents generate multiple aliasing frequencies; a detailed analysis on the strength and weakness of the new high frequency pole model from Desai and Sibois (2016) is beyond the scope of this analysis. Let us conclude, however, that the new model seems to be moderately better than the old one but it is also not free from weaknesses. This conclusion is in line with the final summary of the IERS ad hoc working group (Gipson, 2018; Moore, 2019), which was established to select the recommended high-frequency pole model from a number of candidates.

For completeness, also the combined dual-system solutions have been computed. The two solutions containing GPS (GPS&Galileo; shown in Fig. 5e and GPS&GLONASS; not shown here) are dominated by the characteristics of the GPS-solution. Nevertheless, the magnitude of the peaks (e.g., the 14.8 days period in the Y-component) is reduced in the dual-system solutions with respect to the GPS-only solution because GLONASS and Galileo show both a smaller peak with the new model than GPS in the single-system solutions.

The GLONASS&Galileo dual-system solution (shown in Fig. 5f) is of special interest regarding the conclusion in Scaramuzza et al. (2018) where it was predicted that the combination of two (or more) systems based on three orbital planes have a significant benefit for the ERP estimation. Even if the noise in the low-frequency range (in particular below 10 days) is still slightly higher than in the

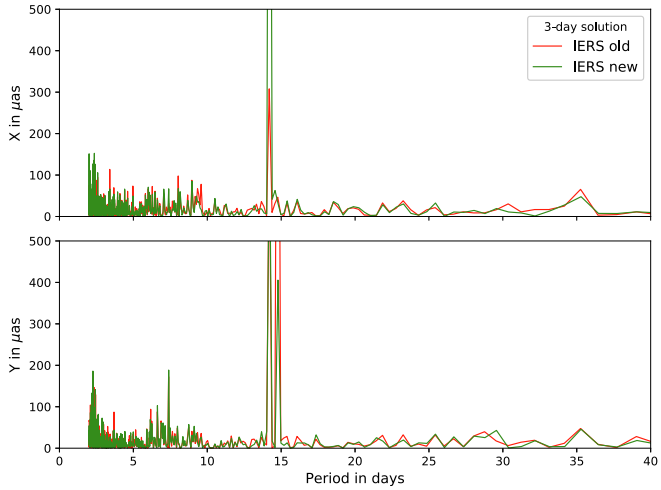

(a) ERP based on all three systems

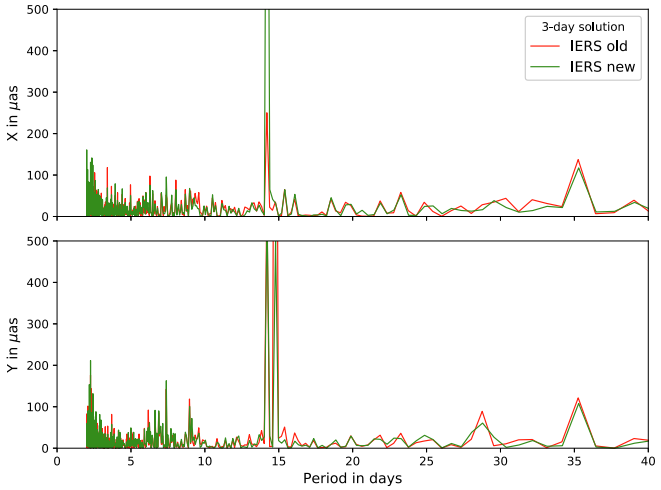

(b) ERP based on GPS only

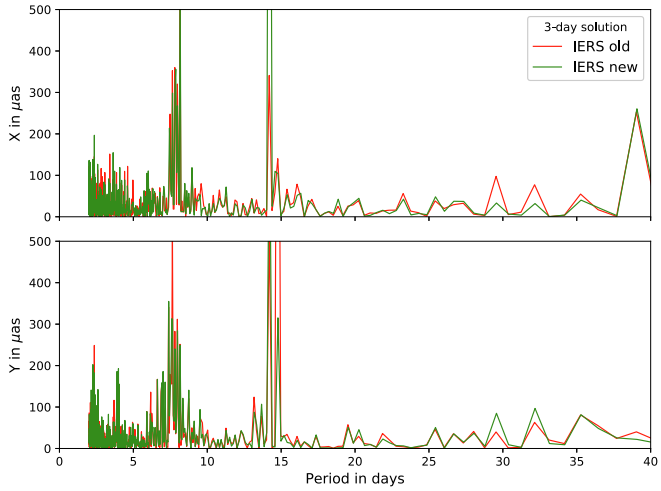

(c) ERP based on GLONASS only

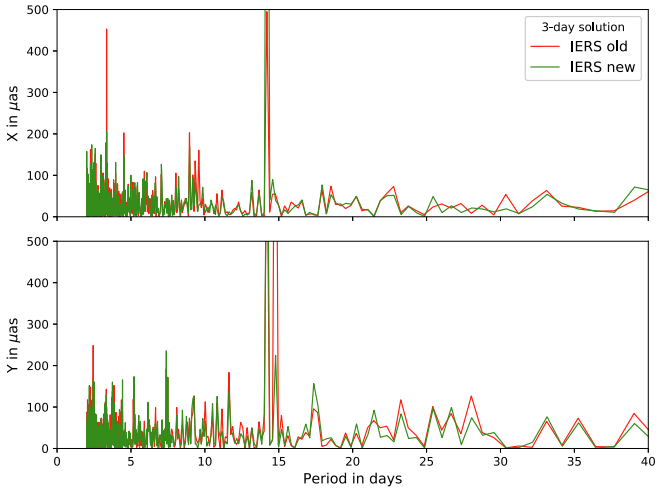

(d) ERP based on Galileo only

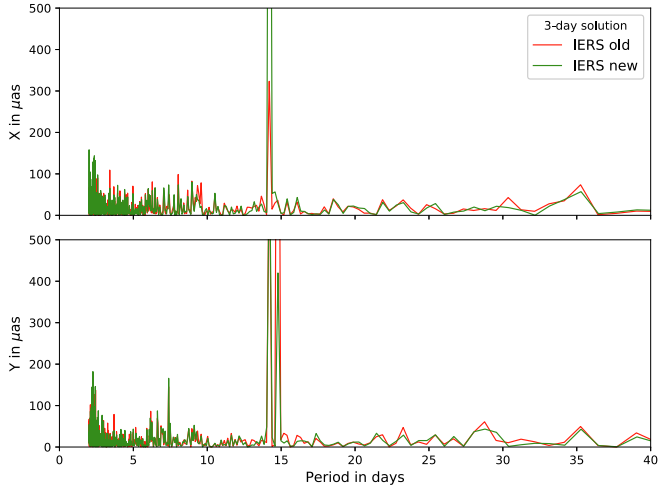

(e) ERP based on GPS&Galileo (without GLONASS)

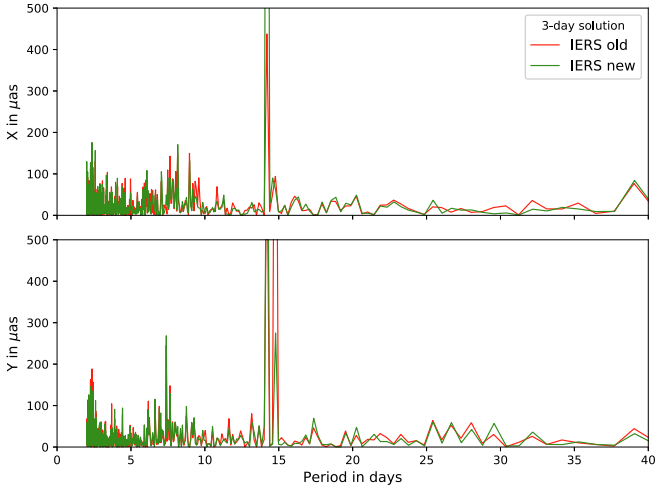

(f) ERP based on GLONASS&Galileo (without GPS)

Fig. 5. Power spectrum of ERP midnight discontinuities based on 3-day GNSS solutions with daily independent ERPs computed for the years 2017 to 2019 where all three models are changed in the new with respect to the old IERS modelling.

GPS-only (Fig. 5b) and the dual-system solutions containing GPS (e.g., Fig. 5e) it is much better than the original single system solutions (see GLONASS in Fig. 5c and Galileo in Fig. 5d).

There is an important difference between a constellation considering of six planes and the combination of two constellations with three planes each. In the six plane constellation of GPS the planes are shifted by 60 degree. In case of three-plane constellations like GLONASS or Galileo, the planes are separated by 120 degree within the constellation. Only if the ascending nodes of the two three plane constellations are shifted by 60 degree, the configuration is comparable to the six plane constellation. At the beginning of the year 2017, the angle between the ascending nodes of the planes from GLONASS and Galileo is about 6 degree only. The value changes in time due to individual nodal precession for each of the systems (in particular because of the bigger inclination of the GLONASS planes) and ends up at 13 degree by end of 2019. It will take about 20 years until these two constellations will have the optimal separation of the orbital planes of 60 degree.

4. Inclusion of Galileo

Apart from the established GNSSs (GPS and GLONASS), the satellite constellation of the European Galileo system was fully deployed by the beginning of 2019, but consists of a reasonable number of satellites already since 2017 (see Fig. 1). First of all, the combination of observations from different GNSS reduce the mapping of satellite orbit-specific frequencies into the products (e.g., investigated by Dach et al., 2009, but later also by many others). In addition the use of the disclosed pre-launch Galileo satellite antenna calibrations (GSA, 2017) offers for the first time the possibility of a potential GNSS contribution to the scale of a reference frame (Villiger et al., 2020). So far, the missing component was the receiver antenna calibration for the new Galileo signal frequencies. This missing link was provided in the course of preparing the IGS reprocessing effort (Wübbena et al., 2019) by establishing a new set of receiver antenna calibrations including all relevant GNSS frequencies.

Prior to this initiative the calibration values for GPS were adopted for Galileo, creating a potential source of inconsistency. While the first frequency agrees among the two GNSS (E1 and L1 at 1.57542 GHz), the second frequency typically used for Galileo analysis (E5a at 1.17645 GHz) is substantially different from the corresponding GPS frequency (L2 at 1.2276 GHz). In order to assess this discrepancy, so called inter-GNSS translation biases (Dach et al., 2015) have been set up in the Bernese GNSS Software package, implicitly meaning that for each of the GNSS separate coordinates are estimated. The geodetic datum definition therefore acts only on the GPS-related coordinates whereas the coordinates for the other systems are attached via a zero-mean condition expressed in the geocentric Cartesian coordinate system. The resulting biases are transformed into the local horizon system at each station where the vertical component is of particular interest in order to study the consistency regarding the scale information and evaluation of the available multi-GNSS receiver antenna calibrations.

Box-plots of the estimated inter-GNSS translation biases during the years 2018 and 2019 are shown in Fig. 6. The stations are sorted according to the antenna used (no distinction regarding the radome is made in order to limit the number of groups). The same station list is used in all panels. This is worth mentioning because in the IGS R3 solutions the GLONASS and Galileo measurements have only been processed if the corresponding receiver antenna corrections have been available (see Section 2). In case of the IGS 14 receiver antenna calibrations such a condition is not applied because copying the GPS-based calibrations to Galileo works in any case. Consequently, these solutions contain more stations where Galileo data are used than the solutions based on the IGS R3 antenna correction model.

The satellite antenna corrections from the IGS 14-related model have been used in Figs. 6a and b. The receiver antenna corrections for GPS and GLONASS measurements are the ones provided for the related systems. On the other hand, for Galileo observations the GPS-based receiver antenna corrections are applied. Systematic biases different from zero result for some antenna types (in particular for Galileo in Fig. 6b). This indicates deficiencies in the practice of using GPS receiver antenna calibrations for Galileo frequencies due to lack of available calibrations. Some of the GLONASS antennas show a similar effect to a lower extent. This may indicate some limitations in the quality of the GLONASS-specific receiver antenna corrections in the IGS 14 model. A similar behavior can be observed also for the horizontal components to a smaller extent. While the largest horizontal inter-GNSS coordinate bias stays below 5 mm the size for the vertical component reaches values of up to 10 mm.

Replacing the receiver antenna model by the new corrections established for each frequency in the multi-GNSS analysis, the biases as presented in Figs. 6c and d result. For GLONASS the systematic biases for some of the antenna types vanish. Only station-specific biases for a few sites remain. In the horizontal components the biases are typically in the range of 1 to 2 mm. The picture for Galileo is comparable for the horizontal components. In the vertical, a mean bias of 7.5 mm results with some variations from station to station.

This is in agreement with the findings of Villiger et al. (2020) where similar biases in the scale with respect to IGS 14 reference frame (the IGS-specific realization of the ITRF 2014, Altamimi et al., 2016) were found, when applying the Galileo satellite antenna corrections together with the new GNSS-specific receiver antenna corrections. Because the GPS and GLONASS satellite antenna corrections have originally been adjusted to the scale of the ITRF 2014 solution but Galileo provides calibrations for

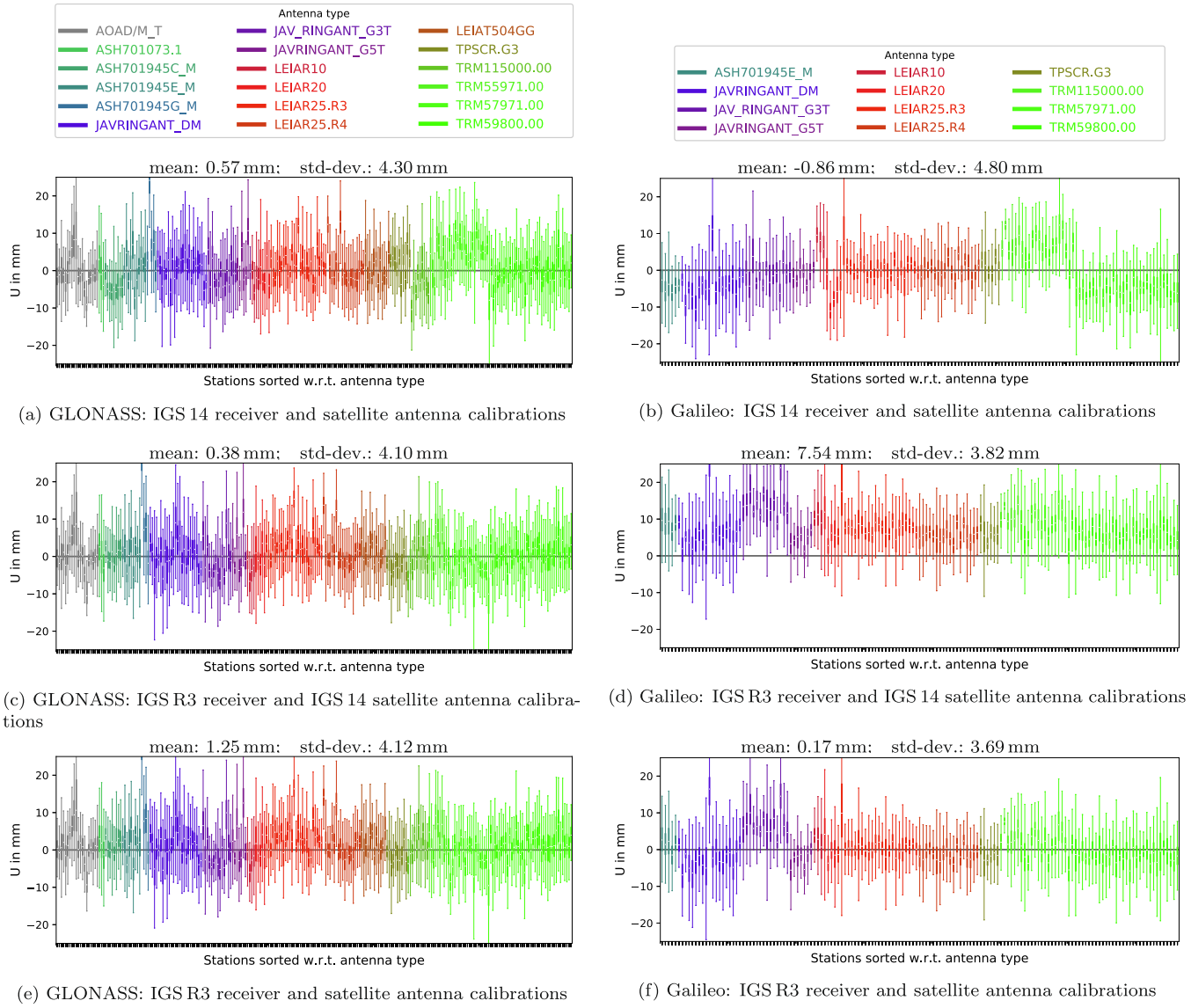

(a) GLONASS: IGS 14 receiver and satellite antenna calibrations

(b) Galileo: IGS 14 receiver and satellite antenna calibrations

(c) GLONASS: IGS R3 receiver and IGS 14 satellite antenna calibrations

(d) Galileo: IGS R3 receiver and IGS 14 satellite antenna calibrations

(e) GLONASS: IGS R3 receiver and satellite antenna calibrations

(f) Galileo: IGS R3 receiver and satellite antenna calibrations

Fig. 6. Box-plots of inter-GNSS translation biases for the vertical component derived from the solutions of the years 2018 and 2019; the colored boxes indicate the interquartile range, the whiskers 1.5 × IQR, the white dot the median. The mean and standard deviation values above the plots are computed from the median values over all stations.

satellite and receiver antennas, it was decided by the IGS ACs to correct the satellite antenna offsets for GPS and GLONASS accordingly by −16.0 cm and −15.6 cm respectively for the current reprocessing effort (Villiger, 2020; Rebischung, 2020). These corrections are included in the IGS R3 antenna model whereas for the Galileo satellites the same antenna corrections are used in all plots of Fig. 6, namely the ones from GSA (2017).

When also for the GPS and GLONASS the corrected satellite antenna offsets (as established in the IGS R3 model) are used together with the new GNSS-specific receiver antenna calibration values, the inter-GNSS translation biases result as shown in Figs. 6e and f. According to the numbers in the plots of Fig. 6, the biases for Galileo and GLONASS have been reduced and the figures are dominated by site-specific effects (apart from the Galileo-related biases for some Javad antennas in violet colors).

From Fig. 6 it can be concluded, that it is harmful to use the correct Galileo-specific receiver antenna corrections in combination with the Galileo satellite antenna corrections as published by GSA (2017) together with the IGS 14 GPS/GLONASS satellite antenna model corrections and the IGS 14 reference frame. The resulting scale discrepancy seems to compensate (by chance) the error introduced into the solution by applying the GPS-based receiver antenna corrections also for the Galileo frequencies.

5. Realization of the three-day orbit solution

CODE has a long tradition in generating long-arc solutions (Beutler et al., 1996), allowing it on the one hand to

mitigate the weakness of the estimated ends of orbital arcs. When generating such a solution based on NEQs as described in Brockmann (1997) none of the observations needs to be processed twice, which speeds up the processing. On the other hand, the resulting length of the long-arc orbit solution is a multiple of the basic processing length of one day, namely 72 h, when adding a daily NEQ before and another one after the day of interest. This arc length is significantly longer than that for other IGS ACs (e.g., 30-h arcs for GRGS or JPL, Perosanz et al., 2020; Murphy et al., 2019).

On the one hand, such long-arc solutions have higher requirements on the representation of the real satellite trajectory by the orbit models. On the other hand, Prange et al. (2016) have demonstrated that there is a significant improvement in the orbit quality for long-arc solutions compared to solutions applying orbit arcs over only one day. This is in particular true for the early period of orbit solutions for the Galileo satellites with a revolution period longer than half a day when the network allowed it only to observe for a part of the satellite revolution. Depending on the satellite and network configuration the satellite may pass the well-observed region (e.g., Europe) only once per day but up to five times in a three-day solution, resulting in a much more reliable estimation of the orbit parameters.

As Lutz et al. (2016) have shown, the longer orbital arcs help to improve the quality of the obtained ERP series. In order to allow for a continuous orbit over the midnight epoch (to be established in the quasi-inertial frame) a continuity condition for the ERP between the consecutive days is needed. On the other hand, a strong continuity condition results in four independent sets of ERPs over 3 days which is not fully compatible with the two sets of ERPs per 24 h as it is usually obtained by the IGS ACs when polar motion and the corresponding rates are computed. In order to overcome this dilemma, the following procedure was implemented in the Bernese GNSS Software and applied for the repro3 for the first time:

- In the daily NEQ the ERPs are given in a piece-wise linear parametrization with two parameters per component at the beginning and the end of each day.
- For a continuity condition when generating multi-day solutions the parameters at midnight can simply be combined into one parameter (which is the traditional approach). Now, these two parameters are kept separate, but constrained to the same estimated ERP value.
- As at the central day boundaries, there are still two parameters per day, they can still be transformed into daily offset and rate per component when generating the SINEX file allowing for two inversions of the NEQ from the SINEX file:
  - with continuity conditions to be fully compatible to the orbit three-day long-arc solution and
  - without continuity condition to be compatible with other ERP representations from other ACs.

With this technical generalization, a compromise between the needs of the IGS and the long-arc solutions favored by CODE was found. So, the CODE contribution to this IGS reprocessing effort is a three-day long arc solution. This circumstance also allows it to reconsider the scheduling of the empirical velocity changes (Beutler et al., 1994), the so called stochastic pulses. In the traditional (e.g., CODE rapid or final) solution, pulses in the three components (radial, along track, out of plane) are set up regularly every twelve hours (at noon and midnight each day) for each satellite. When analyzing the solutions from a previous reprocessing series (e.g., the EGSIEM-reprocessing results documented by Sušnik et al., 2020) it turned out that these pulses have shown the biggest benefit when located in the middle of the period when the satellite is passing the Earth shadow. Most of the other pulses did not have a significant impact on the obtained orbit solution, in particular if the Sun has high elevation above the orbital plane.

This result indicates that the parameters of the Empirical CODE Orbit Model (ECOM, Arnold et al., 2015) are quite efficient to model the GNSS satellite orbits. Since the ECOM parameters are intended to absorb the solar radiation pressure (SRP) effect they are switched off when the satellite is in the Earth (and Moon) shadow. In this period, only the osculating elements are available to compensate for forces acting on the satellite. Since the osculating elements have to represent the orbit through the entire orbital arc, they are unable to compensate for any non-gravitational force during the shadow period (assuming that the gravitational forces are sufficiently modeled).

Sidorov et al. (2020) have demonstrated using the example of the Galileo satellites that the thermal emission from the satellite radiators has a significant influence on the orbit – a force that is also acting during the eclipse phases. With the usual setup there is none of the ECOM parameters available that can compensate for these forces. The generation of a physical model seems currently not possible because of missing publicly available thermal properties information. That the stochastic orbit parameters can absorb such effects was shown for instance by Sidorov et al. (2020) where their magnitude was reduced by enabling the empirical thermal radiation modeling.

Obviously the stochastic pulses may compensate certain orbit modeling deficiencies. It thus seems to be appropriate to schedule the stochastic pulses related to the orbit revolution period, e.g., in the middle of the eclipse period, instead of distributing them equally spaced (every 12 h) over the orbital arc. The use of the stochastic pulses was not limited to the eclipse season but to orbit midnight in general because there was a positive impact observed also for one or two weeks before and the end of the eclipse season (in particular for GLONASS). This new scheme of scheduling the stochastic pulses is applied in the CODE repro3 contribution.

The orbit misclosures with the old and new scheme of scheduling the stochastic orbit parameters are compared

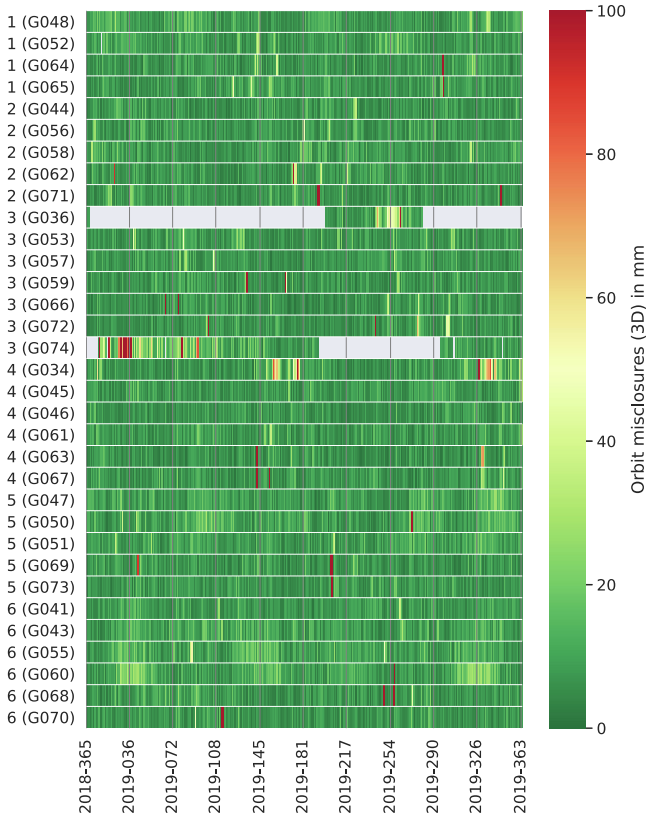

(a) GPS: pulses at noon and midnight

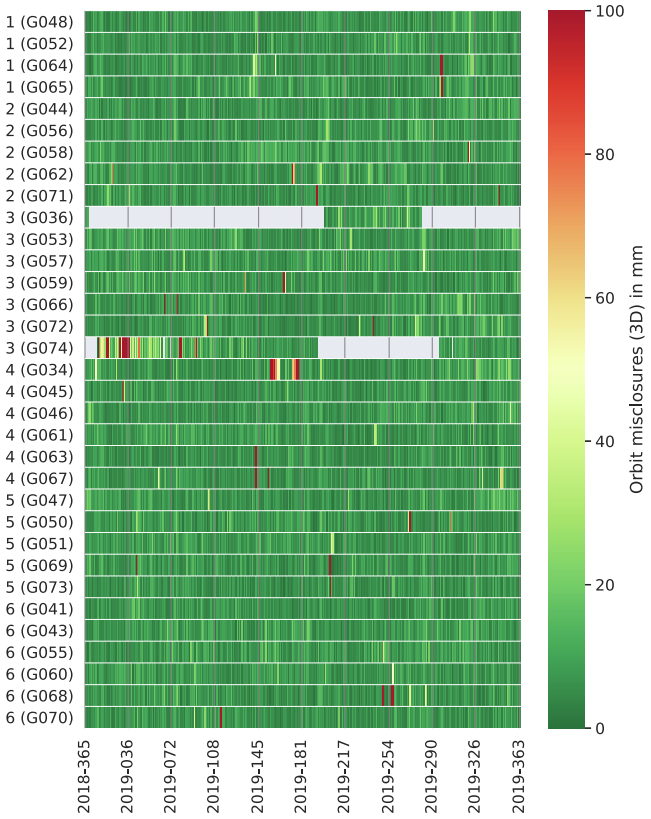

(b) GPS: pulses at orbit midnight

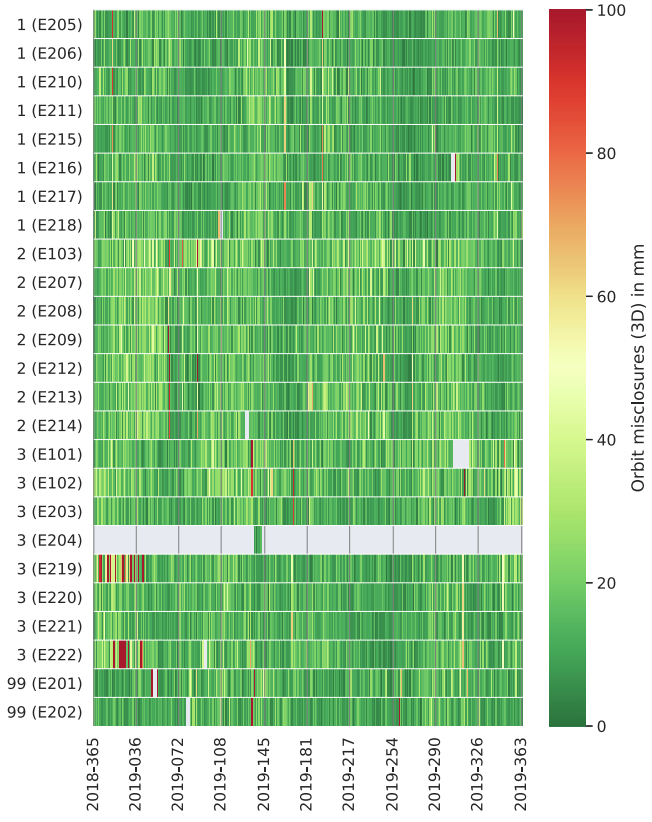

(c) Galileo: pulses at noon and midnight

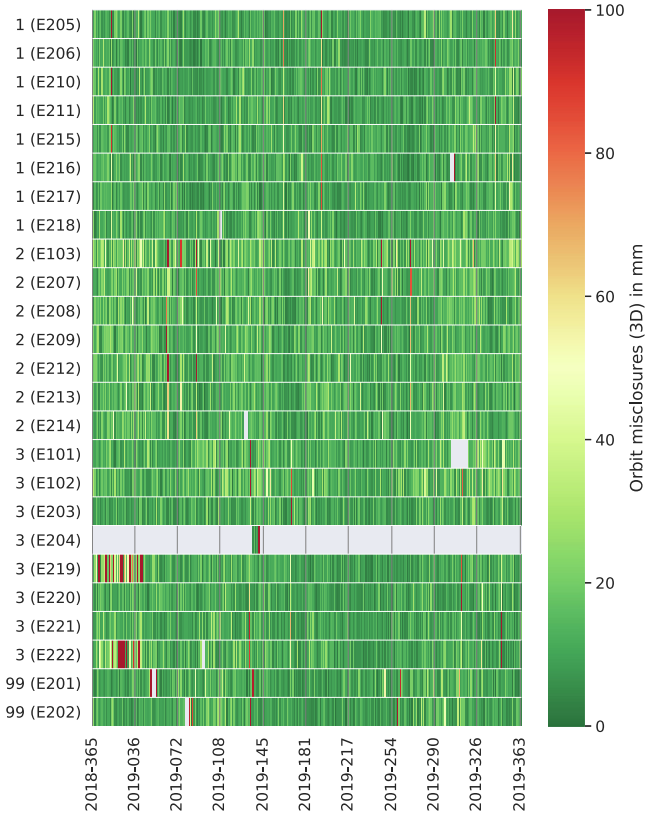

(d) Galileo: pulses at orbit midnight

Fig. 7. Orbit misclosures from three-day solutions in 2019; the satellites are sorted according to the orbital planes (the two Galileo satellites in the elliptic orbit are indicated with the artificial plane number 99); the satellite numbers are the SVN.

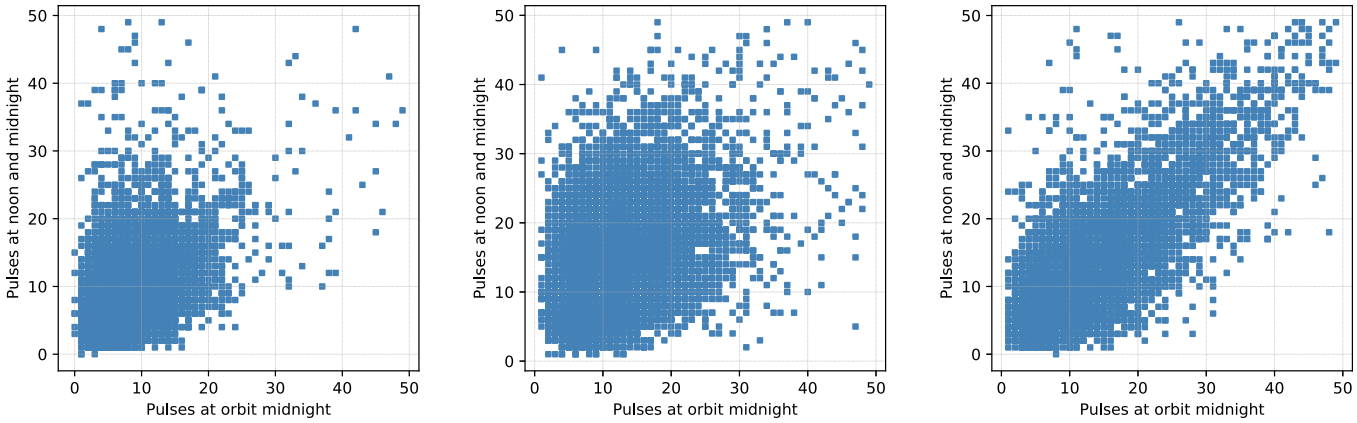

(a) GPS (b) Galileo (c) GLONASS

Fig. 8. Comparisons of orbit misclosures in millimeter from three-day solutions in 2019 between solution with stochastic pulses at noon and midnight with respect to the solution with pulses at orbit midnight.

in Fig. 7 for the GPS and Galileo constellations during the year 2019. In general the yellow structures from the left hand plots (bigger misclosure values from the old scheduling of the pulses) are mostly gone in the right hand plots with the new scheduling. When applying this new scheme, the orbit misclosures for GPS satellites are reduced by about 10% on average. The reduction depends in detail on the satellite type, the biggest benefit resulting for Block IIR-M (SVN range from 48 to 58), to lower extent for Block IIR-B (SVNs 47 and 59 to 61) and nearly no benefit is achieved for Block IIF satellites (SVN range from 62 to 73).

For the Galileo satellites the orbit misclosures improve even by about 15% by rescheduling the epochs of the stochastic pulses, because the orbital revolution period is farther away from the solar day than for GPS. In this way, potential periodic orbit errors are sampled in favor of GPS. In addition, the orbit modeling for Galileo satellites is more sensitive to non-gravitational forces because of the larger area-to-mass ratio. On the other hand, the orbit modeling for Galileo makes use of the published satellite properties (GSA, 2017) as a priori model, a practice that was suggested, e.g., by Bury et al. (2019).

A similar picture is provided by Fig. 8 where the orbit misclosures from both solution series are directly compared. The values from the traditional solution with stochastic pulses at daily noon and midnight are plotted on the axis of the ordinate whereas the misclosures from the solution with the revised scheduling of the stochastic pulses at orbit midnight are plotted on the axis of abscissas. A symbol above the diagonal line means in that way an improvement whereas a point below indicates a degradation.

In case of GPS (Fig. 8a) 54% of the points are in the bin for orbit misclosures below one centimeter with both strategies. This agrees with the conclusion from Fig. 7 that only a subset of the satellite types really benefits from the changed scheduling of the stochastic pulses. There are 17% where the magnitude can be reduced from between one and two centimeters below one centimeter but also 10% where an increase from below one towards a range of between one and two centimeters appears. Overall, 10% of the orbit misclosures do not change and 52% are reduced by the rescheduling of the stochastic pulses.

The situation with GLONASS is not that clear. On one hand, completely removing the stochastic pulses from the processing, shows that they are beneficial not only in the eclipse seasons, but even one to three weeks before and after this interval (Dach et al., 2018). It looks like these satellites change their attitude maintenance scheme (mentioned as "eclipse passing algorithm" in Dilssner et al., 2011) a certain time before and after the eclipse season. This is another reason to setup the pulses at orbit midnight also outside the eclipse season. On the other hand, Fig. 8c shows that there is nearly no effect on the orbit misclosures from the scheduling of the stochastic pulses for the GLONASS satellites. This was also already documented in Dach et al. (2018). Obviously the orbit modeling for these satellites do suffer from other effects where for instance Dach et al. (2019) has reported one of them – even if the alternative satellite antenna corrections have been applied in the solutions discussed here (in contrast to Dach et al., 2018).

With this rescheduled stochastic pulses the average of the orbit misclosures for the Galileo constellation is at least on the same level as for GLONASS (12.8 mm and 12.5 mm respectively). With the pulses at noon and midnight the misclosures have a magnitude of 14.8 mm for Galileo and 12.7 mm for GLONASS. The corresponding numbers of GPS show a reduction from 8.8 mm to 7.8 mm.

This effect may be seen as a CODE-specific issue because the long-arc solution is more sensitive to unmodeled orbit effects. For a further refinement of the GNSS satellite orbit modeling one needs dedicated orbit model studies during the eclipse period – preferably of course based on publicly available information about the satellites. A comparison of

the CODE orbits with the orbits provided by other IGS ACs reveals no specific orbit degradation during the eclipse seasons. This result implies that other groups are affected by the same problems.

6. Downweighting observations of misbehaving satellites

Springer (2000) reported a set of GPS satellites with a reduced attitude stability towards the end of the 1990s. He lists up to seven satellites with potential issues for September 1998 in Table 2.1 (Springer, 2000): PRNs 14 and 16 are indicated with "Wheels" as well as PRNs 18, 19, 24 and 29 with "Wheels?" (for all these satellites the PRNs and SVNs are identical at that time). These satellites are explained to have problems with their momentum wheels needed for attitude stabilization. For PRN/SVN 23 ("Panel") the attitude stability is also limited because the solar panel adjustment could not be carried out by the usual automatic procedure.

These problem satellites represent at that time about a quarter of the entire active GPS constellation. They were in use partially even through to the mid of the 2000s, implying that they may affect about the first third of the reprocessing period. Consequently, for a reprocessing effort (here in particular repro3) a special treatment is needed for these satellites because they also showed a reduced orbit quality (e.g., indicated by higher values for the orbit misclosures) in previous reprocessing efforts.

In order to identify the related periods two consecutive daily orbit arcs are represented by one two-day arc. The two-day arc is compared to the two original orbits in terms of 3D-RMS of satellite positions every 15 min for each satellite (σ_{sat}). A mean RMS for the entire GPS constellation is computed (σ_{GPS}). A satellite is indicated as potentially problematic if the satellite-specific RMS exceeds a limit of four times the mean RMS over the entire constellation ($\sigma_{sat} > 4 \cdot \sigma_{GPS}$). If a sequence of such indications (at least 15 out of 20 days) is detected a potentially problematic satellite is assumed. In such a case also the estimated SRP coefficients have been inspected more closely because they also typically show an "unusual pattern" in case of serious orbit modelling problems.

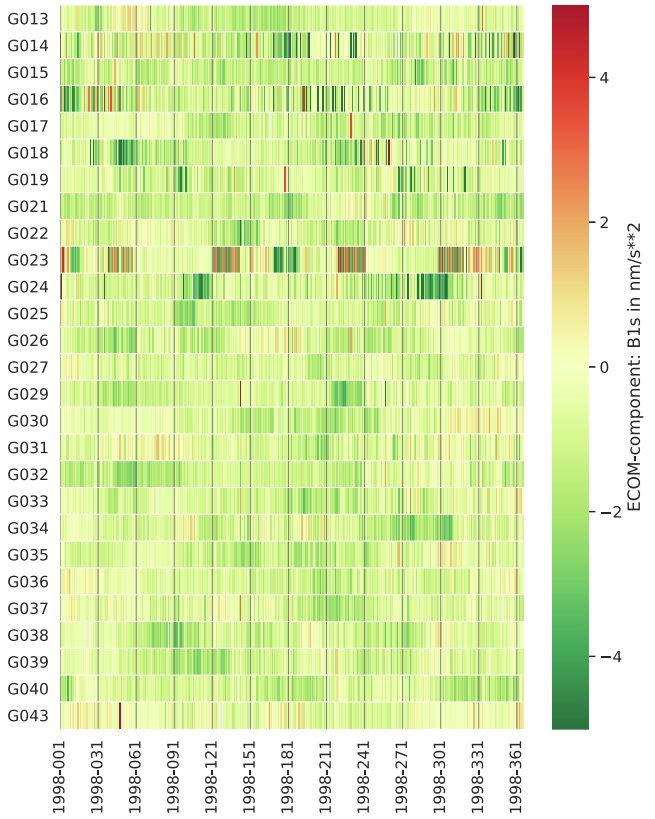

Fig. 9. Estimated sine terms for the once-per-revolution component in B direction of the ECOM decomposition according to Arnold et al. (2015) for the GPS satellites during the year 1998; the satellites are sorted by their SVN.

Fig. 9 shows the estimated SRP coefficients for the sine component in B-direction as an example. They are typically in the range of $\pm 2\,\mathrm{nm/s^2}$. For some satellites this range is exceeded during several periods of the year, namely for SVNs 14, 16, 23, and 24. The same satellites were marked by Springer (2000) to have problems with attitude maintenance. Also the test with the long-arc fit described in the previous paragraph did indicate potential problems for the same satellites. Therefore, these estimated SRP parameters were used as complementary information when interpreting a cumulation of large RMS values in the two-day arcs. Based on this information, the periods with problem-

Table 3
Time periods when the observations to specific GPS-satellites have been downweighted because of modeling problems.

SVN/PRN		satellite active		downweighted	
13	02	1989–06-10	2004–05-13	2001–04-10	2003–06-03
14	14	1989–02-14	2000–04-16	1996–05-16	2000–04-16
15	15	1990–10-01	2007–03-14	1999–04-21	2003–01-02
16	16	1989–08-18	2000–10-14	1996–02-08	2000–10-14
17	17	1989–12-11	2005–02-24	2000–12-03	2003–07-16
18	18	1990–01-24	2000–08-19	1996–05-12	2000–08-19
19	19	1989–10-21	2001–09-12	1996–04-29	2001–09-12
21	21	1990–08-02	2003–01-28	2000–12-31	2003–01-28
23	23	1990–11-26	2004–02-17	1995–02-01	2002–01-02
24	24	1991–07-04	2011–10-01	1997–11-15	2004–07-11
29	29	1992–12-18	2007–10-24	2001–12-02	2007–10-24

atic attitude behavior of the GPS satellites were identified and listed in Table 3.

All GPS satellites with attitude stability problems were launched before 1992. Almost the complete fleet of Block II satellites (SVNs between 13 and 21) is in the list; except for PRN20/SVN20, which was deactivated after only six years of service. From the Block IIA generation, 6 satellites were launched in 1992 (SVNs 25 to 29, and 32). Only three of them (SVNs 23, 24, and 29) are affected. Overall, eleven satellites are affected, the largest simultaneous number is eight (out of 28 active GPS satellites) in 1999 and at the beginning of the year 2000. The last satellite with this kind of problems was deactivated in October 2007 (SVN 29). Some of the satellites returned to nominal behavior (SVNs 13, 15, 17, 23, and 24) after some months/years of the degraded service.

For the reprocessing observations to these satellites were downweighted by a factor of 10 during the time periods listed in Table 3. This prevented a contamination of the global solutions by these problematic satellites. To illustrate this, Fig. 10 shows the orbit misclosures for all GPS satellites for the year 2000 with and without downweighting. The effect of the attitude instability propagates differently depending on the elevation of the Sun above the orbital plane. As the affected satellites are located only in some of the orbital planes, the amount of orbit degradation for the other satellites is varying. There are time periods where most of the satellites affected by attitude instability (up to a third of all satellites) lie in orbital planes with low Sun elevation angle. Including observations to these satellites with equal weight then results in an obvious degradation of orbit quality for the entire constellation. If, on the other hand, the mentioned satellite-specific weighting scheme is applied, this orbit degradation is restricted to the satellites with attitude problems. For those satellites the orbit misclosures slightly increase which is expected in a least squares adjustment.

Downweighting observations to misbehaving satellites not only improves the general orbit quality, but also the quality of other estimated parameters. This is in particular true for the ERPs during the time periods when all orbit parameters are degraded in Fig. 10a. The differences with respect to the C04 series from the IERS are more consistent. The power spectra of the X- and Y-components of polar motion in Fig. 11 document a significant reduction of spurious spectral lines when downweighting the observations of the satellites in Table 3. The time period 1997–2002 was analyzed in Fig. 11 because a significant part of the GPS constellation was affected in this period.

Similar improvements also result for the station coordinates. When comparing the estimated coordinates with those given in the reference frame the RMS of a Helmert transformation can be taken as a quality measure. This value becomes more consistent in time (i.e., shows less sys-

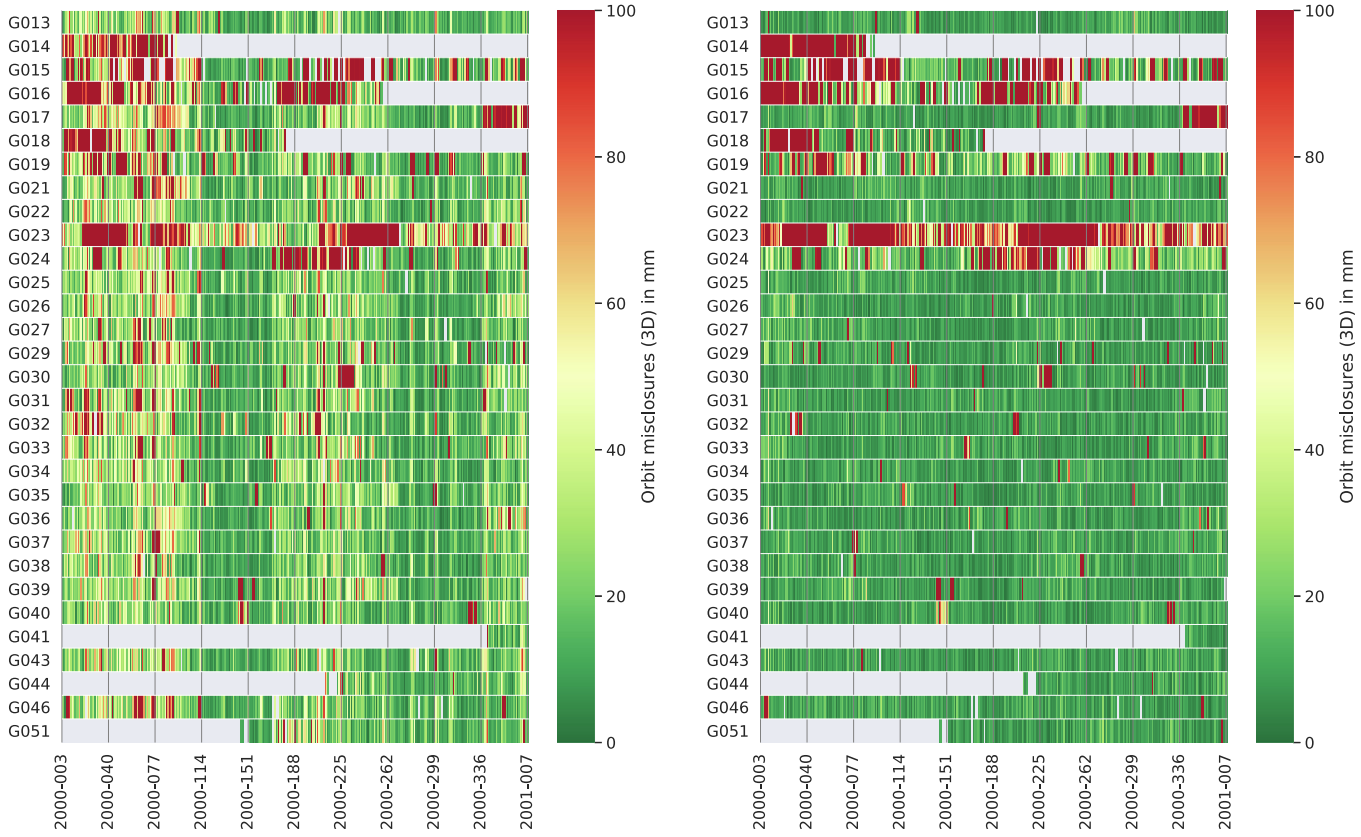

(a) all satellites with the same weight

(b) downweighting of degraded satellites enabled

Fig. 10. Orbit misclosures from three-day solutions during the year 2000; the satellites are sorted according to their SVN.

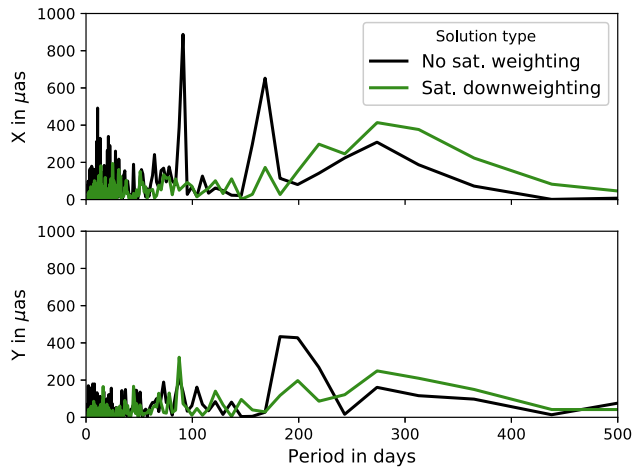

Fig. 11. Power spectrum of the differences between the estimated polar motion series and the reference series (IERS 14C04) for 1997–2002.

tematic variations) in particular during the 1990s and the early 2000s when applying the downweighting scheme for the misbehaving satellites. Even if downweighting the satellites means that the solution is computed in fact by fewer observations for global and station-related parameters. Obviously this reduction is less harmful to the solution than the inclusion of satellites with reduced orbit quality due to the uncertainty of the attitude stability.

7. Summary and Conclusions

CODE contributes with a multi-GNSS solution to the repro3 – the third reprocessing effort of the IGS. This solution is derived from the operational CODE final product generation scheme by applying various model changes and improvements.

Selected IERS conventional and background models were updated, namely the mean pole model and the high-frequency pole model (Desai and Sibois, 2016). Also the ocean tide model was changed from FES2004 to FES2014b for modeling ocean tidal loading station displacement and to include the gravitational influence on the GNSS satellite orbits. Because there are aliasing effects between the periods of tidal constituents and the orbit revolution periods, the effect of the model change is expected to have different magnitude for each GNSS. When comparing the GNSS-specific ERP discontinuities between the estimates for consecutive days at midnight, it turns out that the amplitudes of a number of spectral lines are reduced. There are also a few examples of an increase of amplitudes. This suggests that the new models seem to be better than their predecessors, but are not perfect.

Galileo was included as the third GNSS in CODE's repro3 contribution. It turned out that the current configuration (as it is used for instance in the CODE-rapid processing) produces a good approximation of the scale as currently established in the IGS 14 frame. In this configuration the Galileo pre-launch satellite antenna calibrations are used whereas for the ground stations the antenna corrections for the two GPS frequencies are also used for the Galileo measurements. When using the updated set of calibrations for the receiver antennas which are including corrections for the Galileo frequencies, a scale offset with respect to IGS 14 frame is obtained, which is compensated by the modified antenna z-offsets for GPS and GLONASS satellites and the reference frame as it is recommended to be used for the IGS reprocessing. The scale for the ground stations becomes again consistent between Galileo and GPS/GLONASS. At the same time some deficiencies in the GNSS-specific receiver antenna calibration did improve as well meaning the inter-GNSS translation biases become smaller. It seems that two independent effects compensate each other to a large extent. When using the IGS 14 reference frame together with the pre-launch satellite antenna calibrations for Galileo, the traditional strategy of using the receiver antenna calibrations from GPS also for Galileo measurements should be applied. GNSS-specific receiver antenna calibrations should only be used together with the updated satellite antenna correction set as prepared by the IGS for repro3 (IGS R3).

As Galileo has a longer revolution period than GPS (approx. $14^h\ 05^m$ compared to $11^h\ 58^m$) the satellites do not complete two revolutions per day. For that reason longer than one-day orbital arcs are preferable as realized by the CODE reprocessing solution with its three-day orbit solutions. On the other hand, longer arcs require a better modeling of the forces acting on the satellites. Even with an a priori force model based on the satellite information as provided by GSA (2017), the satellite trajectory cannot be represented on the centimeter level if the usual empirical ECOM2 parameters are estimated. Empirical velocity changes absorb a part of the unmodelled effects in the satellite orbits. These so-called stochastic pulses have been rescheduled from an uniform spacing in the operational CODE solution (every 12 h at noon and midnight) to the orbit midnight epoch. Due to this more reasonable scheduling the orbit misclosures at midnight are reduced by 10% for GPS and even by 15% for Galileo satellites, in particular during the eclipse season. This improvement indicates weaknesses in the orbit modelling during the eclipse season. Comparing the CODE orbits with those from other IGS ACs does not indicate a degradation of the CODE orbit products during eclipse season confirming the consistency of all AC solutions also during this period. This implies that this particular issue is not CODE-specific.

Last but not least, time periods between 1995 and 2007 have been identified when some of the GPS satellites suffer from persisting attitude control problems. This degrades some of the estimated SRP parameters, thus, reducing the orbit quality for the affected satellites. Other parameters of the solutions may be degraded, as well, as a consequence of the attitude problems – in particular between 1999 and 2001 when about a quarter of the active GPS satellites is affected. By downweighting of the measure-

ments of these satellites the resulting time series are significantly improved.

8. Availability of the reprocessed product files

The CODE contribution to the recent reprocessing effort of the IGS includes:

- GPS: orbits since 1994; satellite clock corrections with 30 s sampling since the year 2000 and starting in the year 2003 even with a 5 s sampling.
- GLONASS: orbits since 2002, satellite clock corrections since 2008 with 30 s and 2011 with 5 s sampling (since year 2012 nearly every day complete).
- Galileo: orbits since 2013; satellite clock corrections since 2014 with 30 s sampling (due to the excellent stability of the satellite clocks no further densification is necessary, linear interpolation between 30 s values is sufficient).

Besides the satellite clock corrections, a consistent set of phase biases is generated, allowing for ambiguity resolution for Precise Point Positioning (PPP) applications following the approach described in Schaer et al. (2020).

The results are made available in the usual international formats at ftp://ftp.aiub.unibe.ch/REPRO_2020/CODE (the detailed list of files is given in A). The dataset is allocated to the DOI: 10.7892/boris.135946.

Declaration of Competing Interest

The authors declare that they have no known competing financial interests or personal relationships that could have appeared to influence the work reported in this paper.

Acknowledgments

Calculations were performed on UBELIX (http://www.id.unibe.ch/hpc), the High Performance Computing (HPC) cluster at the University of Bern.

Appendix A. List of available product files from the CODE repro3 solution

Files generated from three-day solutions and made available at ftp://ftp.aiub.unibe.ch/REPRO_2020/CODE:

Ephemeris
`COD0R03FIN_yyyyddd0000_01D_05M_ORB.SP3`
GNSS ephemeris/clock data in daily files at 5-min intervals in SP3d format, including accuracy codes computed from a long-arc analysis

Daily ERPs
`COD0R03FIN_yyyyddd0000_01D_01D_ERP.ERP`
GNSS ERP (pole, UT1-UTC) solution in IGS ERP format

Normal equation
`COD0R03FIN_yyyyddd0000_01D_01D_SOL.SNX`
GNSS daily coordinates and ERP parameters together with geocenter coordinates and satellite antenna phase center offset parameters from the long-arc solution in SINEX 2.01 format

Clocks, 30s
`COD0R03FIN_yyyyddd0000_01D_30S_CLK.CLK`
GNSS satellite and receiver clock corrections at 30-s intervals referring to the CODE-orbits from the long-arc analysis in clock RINEX 3.04 format

Clocks, 5s
`COD0R03FIN_yyyyddd0000_01D_05S_CLK.CLK`
GNSS satellite and receiver clock corrections at 5-s intervals referring to the CODE-orbits from the long-arc analysis in clock RINEX 3.04 format

Code & Phase bias
`COD0R03FIN_yyyyddd0000_01D_01D_OSB.BIA`
CODE daily code and phase bias solution corresponding to the above mentioned clock products in BIAS-SINEX 1.00 format

Weekly ERPs
`COD0R03FIN_yyyyddd0000_07D_01D_ERP.ERP`
GNSS ERP (pole, UT1-UTC) solution, collection of the 7 daily COD-ERP solutions of the week in IGS ERP format; labeled with the starting day of the week

Weekly summary
`COD0R03FIN_yyyyddd0000_07D_07D_SUM.SUM` Analysis summary for 1 week on the long-arc solutions of the week; labeled with the starting day of the week

The files are provided in yearly subdirectories. The abbreviation `yyyyddd` in the above listed filenames stands for the 4-digit year and the day of year.

References

Abraha, K., Teferle, F., Hunegnaw, A., Dach, R., 2018. Effect of unmodelled tidal displacements in GPS and GLONASS coordinate time series. Geophys. J. Int. 214 (3), 2195–2206. https://doi.org/10.1093/gji/ggy254.

Altamimi, Z., Rebischung, P., Métivier, L., Collilieux, X., 2016. ITRF2014: A new release of the International Terrestrial Reference Frame modeling nonlinear station motions. J. Geophys. Res. 121 (8), 6109–6131. https://doi.org/10.1002/2016JB013098.

Arnold, D., Meindl, M., Beutler, G., Dach, R., Schaer, S., Lutz, S., Prange, L., Sośnica, K., Mervart, L., Jäggi, A., 2015. CODE's new solar radiation pressure model for GNSS orbit determination. J. Geodesy 89 (8), 775–791. https://doi.org/10.1007/s00190-015-0814-4.

Bassiri, S., Hajj, G., 1993. Higher-order ionospheric effects on the Global Positioning System observables and means of modeling them. Manuscripta Geodaetica 18, 280–289.

Beutler, G., Brockmann, E., Gurtner, W., Hugentobler, U., Mervart, L., Rothacher, M., Verdun, A., 1994. Extended orbit modeling techniques at the CODE processing center of the International GPS Service for Geodynamics (IGS): Theory and initial results. Manuscripta Geodaetica 19 (6), 367–386.

Beutler, G., Brockmann, E., Hugentobler, U., Mervart, L., Rothacher, M., Weber, R., 1996. Combining consecutive short arcs into long arcs for precise and efficient GPS orbit determination. J. Geodesy 70 (5), 287–299. https://doi.org/10.1007/BF00867349.

Bizouard, C., Lambert, S., Gattano, C., Becker, O., Richard, J.Y., 2019. The IERS EOP 14C04 solution for Earth orientation parameters consistent with ITRF 2014. J. Geodesy 93 (5), 621–633. https://doi.org/10.1007/s00190-018-1186-3.

Bock, H., Dach, R., Jäggi, A., Beutler, G., 2009. High-rate GPS clock corrections from CODE: support of 1 Hz applications. J. Geodesy 83 (11), 1083–1094. https://doi.org/10.1007/s00190-009-0326-1.

Böhm J, Schuh H (2004) Vienna mapping function in VLBI analyses. Geophys. Res. Lett. 31(1):L01,603, doi:10.1029/2003GL018984

Brockmann E (1997) Combination of solutions for geodetic and geodynamic applications of the Global Positioning System (GPS). In: Geodätisch-geophysikalische Arbeiten in der Schweiz, vol 55, Schweizerische Geodätische Kommission, Institut für Geodäsie und Photogrammetrie, Eidg. Technische Hochschule Zürich, Zürich.

Brunner, F.K., Gu, M., 1991. An improved model for dual frequency ionospheric correction of GPS observations. Manuscripta Geodaetica 16 (3), 205–214.

Bury, G., Zajdel, R., Sośnica, K., 2019. Accounting for perturbing forces acting on Galileo using a box-wing model. GPS Solutions 23 (3), 74. https://doi.org/10.1007/s10291-019-0860-0.

Carrere L, Lyard F, Cancet M, Guillot A, Picot N (2016) FES 2014, a new tidal model – validation results and perspectives for improvements. In: ESA LivingPlanet Conference, Prague 2016.

Chen G, Herring TA (1997) Effects of atmospheric azimuthal asymmetry on the analysis of space geodetic data. J. Geophys. Res. 102 (B9):20,489–20,502, doi:10.1029/97JB01739

Dach, R., Brockmann, E., Schaer, S., Beutler, G., Meindl, M., Prange, L., Bock, H., Jäggi, A., Ostini, L., 2009. GNSS processing at CODE: Status report. J. Geodesy 83 (3–4), 353–365. https://doi.org/10.1007/s00190-008-0281-2.

Dach R, Lutz S, Walser P, Fridez P (eds) (2015) Bernese GNSS Software, Version 5.2. Astronomical Institute, University of Bern, Bern, Switzerland, doi:10.7892/boris.72297, ftp://ftp.aiub.unibe.ch/BERN52/DOCU/DOCU52.pdf, user manual.

Dach R, Bachmann N, Sušnik A, Villiger A, Arnold D, Jäggi A (2018) Evaluating orbits from the egsiem reprocessing. In: EGU General Assembly 2018, 08-13 April 2018, Vienna, Austria

Dach, R., Sušnik, A., Grahsl, A., Villiger, A., Schaer, S., Arnold, D., Prange, L., Jäggi, A., 2019. Improving GLONASS orbit quality by re-estimating satellite antenna offsets. Adv. Space Res. 63 (12), 3835–3847. https://doi.org/10.1016/j.asr.2019.02.031.

Dach R, Schaer S, Arnold D, Prange L, Sidorov D, Stebler P, Villiger A, Jäggi A, Beutler G, Brockmann E, Ineichen D, Lutz S, Wild U, Nicodet M, Dostal J, Thaller D, Söhne W, Bouman J, Selmke I, Hugentobler U (2020) CODE Analysis center: IGS Technical Report 2019. In: Villiger A, Dach R (eds) International GNSS Service: Technical Report 2019, IGS Central Bureau, pp 39–56.

Desai, S.D., Sibois, A.E., 2016. Evaluating predicted diurnal and semidiurnal tidal variations in polar motion with GPS-based observations. J. Geophys. Res. 121 (7), 5237–5256. https://doi.org/10.1002/2016JB013125.

Dilssner, F., Springer, T., Gienger, G., Dow, J., 2011. The GLONASS-M satellite yaw-attitude model. Adv. Space Res. 47 (1), 160–171. https://doi.org/10.1016/j.asr.2010.09.007.

Fritsche, M., Sośnica, K., Rodriguez-Solano, C., Steigenberger, P., Wang, K., Dietrich, R., Dach, R., Hugentobler, U., Rothacher, M., 2014. Homogeneous reprocessing of GPS, GLONASS and SLR observations. J. Geodesy 88 (7), 625–642. https://doi.org/10.1007/s00190-014-0710-3.

Gipson J (2018) IERS Working Group on HF-EOP. In: AGU Fall Meeting 2018, 10-14 December 2018, Washington, D.C., USA

GSA (2017) Galileo satellite metadata. https://www.gsc-europa.eu/support-to-developers/galileo-satellite-metadata, last access: 31 Oct. 2019.

Johnston, G., Riddell, A., Hausler, G., 2017. The International GNSS Service. In: Teunissen, P., Montenbruck, O. (Eds.), Springer Handbook of Global Navigation Satellite Systems. Springer International Publishing, Cham, Switzerland, pp. 967–982. https://doi.org/10.1007/978-3-319-42928-1.

King, M.A., Watson, C.S., 2014. Geodetic vertical velocities affected by recent rapid changes in polar motion. Geophys. J. Int. 199 (2), 1161–1165. https://doi.org/10.1093/gji/ggu325.

Kouba, J., 2003. Testing of the IERS2000 sub-daily Earth rotation parameter model. Stud Geophys Geod 47, 725–739. https://doi.org/10.1023/A:1026338601516.

Kouba, J., 2009. A simplified yaw-attitude model for eclipsing GPS satellites. GPS Solutions 13 (1), 1–12. https://doi.org/10.1007/s10291-008-0092-1.

Lutz, S., Meindl, M., Steigenberger, P., Beutler, G., Sośnica, K., Schaer, S., Dach, R., Arnold, D., Thaller, D., Jäggi, A., 2016. Impact of the arc length on GNSS analysis results. J. Geodesy 90 (4), 365–378. https://doi.org/10.1007/s00190-015-0878-1.

Lyard, F., Lefevre, F., Letellier, T., Francis, O., 2006. Modelling the global ocean tides: insights from FES2004. Ocean Dyn. 56, 394–415. https://doi.org/10.1007/s10236-006-0086-x.

Montenbruck, O., Steigenberger, P., Prange, L., Deng, Z., Zhao, Q., Perosanz, F., Romero, I., Noll, C., Stürze, A., Weber, G., Schmid, R., MacLeod, K., Schaer, S., 2017. The Multi-GNSS Experiment (MGEX) of the International GNSS Service (IGS) – Achievements, prospects and challenges. Adv. Space Res. 59 (7), 1671–1697. https://doi.org/10.1016/j.asr.2017.01.011, article.

Moore M (2019) Workshop recommendations. In: IGS Analysis Center Workshop 2019, 15-17 April 2019, Potsdam, Germany, URL https://s3-ap-southeast-2.amazonaws.com/igs-acc-web/igs-acc-website/workshop2019/Workshop_Findings.pdf.

Murphy D, Bertiger W, Dietrich A, Hemberger D, Ries P, Sibois A, Sibthorpe A (2020) JPL Analysis center: IGS Technical Report 2019. In: Villiger A, Dach R (eds) International GNSS Service: Technical Report 2019, IGS Central Bureau, pp 89–94.

Penna, N., King, M., Stewart, M., 2007. GPS height time series: Short-period origins of spurious long-period signals. J. Geophys. Res. 112 (B2). https://doi.org/10.1029/2005JB004047.

Perosanz F, Loyer S, Mercier F, Katsigianni G, Mezerette A, Garcia AB, Capdeville H, J CM, Santamaria A (2020) CNES-CLS Analysis center: IGS Technical Report 2019. In: Villiger A, Dach R (eds) International GNSS Service: Technical Report 2019, IGS Central Bureau, pp 83–88.

Petit G, Luzum B (2010) IERS Conventions (2010). IERS Technical Note 36, Bundesamt für Kartographie und Geodäsie, Frankfurt am Main, URL http://www.iers.org/IERS/EN/Publications/TechnicalNotes/tn36.html.

Prange L, Dach R, Lutz S, Schaer S, Jäggi A (2016) The CODE MGEX orbit and clock solution. In: Rizos C, Willis P (eds) IAG 150 Years, Springer, International Association of Geodesy Symposia, vol 143, pp 767–773, doi:10.1007/1345_2015_161.

Rebischung, P., 2020. Refernce frame working group technical report 2019. In: Villiger, A., Dach, R. (Eds.), International GNSS Service: Technical Report 2019. IGS Central Bureau, pp. 237–246.

Rodriguez-Solano, C.J., Hugentobler, U., Steigenberger, P., Lutz, S., 2012. Impact of Earth radiation pressure on GPS position estimates. J. Geodesy 86 (5), 309–317. https://doi.org/10.1007/s00190-011-0517-4.

Scaramuzza, S., Dach, R., Beutler, G., Arnold, D., Sušnik, A., Jäggi, A., 2018. Dependency of geodynamic parameters on the GNSS constellation. J. Geodesy 92 (1), 93–104. https://doi.org/10.1007/s00190-017-1047-5.

Schaer, S., Villiger, A., Arnold, D., Dach, R., Prange, L., Jäggi, A., 2020. The CODE ambiguity-fixed clock and phase bias analysis products: generation, properties, and performance. JJ. Geodesy. Manuscript in review.

Sidorov, D., Dach, R., Polle, B., Prange, L., Jäggi, A., 2020. Adopting the empirical CODE orbit model to Galileo satellites. Adv. Space Res. 66 (12), 2799–2811. https://doi.org/10.1016/j.asr.2020.05.028.

Springer TA (2000) Modeling and validating orbits and clocks using the Global Positioning System. Geodätisch-geophysikalische Arbeiten in der Schweiz, vol 60, Schweizerische Geodätische Kommission, Institut für Geodäsie und Photogrammetrie, Eidg. Technische Hochschule Zürich, Zürich.

Steigenberger P, Lutz S, Dach R, Hugentobler U (2011) CODE contribution to the first IGS reprocessing campaign. Tech. rep., Technische Universität München

Steigenberger P, Lutz S, Dach R, Schaer S, Jäggi A (2014) CODE repro2 product series for the IGS. doi:10.7892/boris.75680, http://www.aiub.unibe.ch/download/REPRO_2013.

Stewart, M., Penna, N., Lichti, D., 2005. Investigating the propagation mechanism of unmodelled systematic errors on coordinate time series estimated using least squares. J. Geodesy 79 (8), 479–489. https://doi.org/10.1007/s00190-005-0478-6.

Sušnik, A., Grahsl, A., Arnold, D., Villiger, A., Dach, R., Beutler, G., Jäggi, A., 2020. Validation of the EGSIEM-REPRO GNSS orbits and satellite clock corrections. Remote Sensing 12 (14), 2322. https://doi.org/10.3390/rs12142322.

Villiger, A., 2020. Antenna working group technical report 2019. In: Villiger, A., Dach, R. (Eds.), International GNSS Service: Technical Report 2019. IGS Central Bureau, pp. 185–194.

Villiger, A., Schaer, S., Dach, R., Prange, L., Sušnik, A., Jäggi, A., 2019. Determination of GNSS pseudo-absolute code biases and their long-term combination. J. Geodesy 93 (9), 1487–1500. https://doi.org/10.1007/s00190-019-01262-w.

Villiger, A., Dach, R., Schaer, S., Prange, L., Zimmermann, F., Kuhlmann, H., Wübbena, G., Schmitz, M., Beutler, G., Jäggi, A., 2020. GNSS scale determination using calibrated receiver and Galileo satellite antenna patterns. J. Geodesy 94, 1394–1432. https://doi.org/10.1007/s00190-020-01417-0.

Willis P, Slater J, Beutler G, Gurtner W, Noll C, Weber R, Neilan RE, Hein G (2000) The IGEX-98 campaign: Highlights and perspective. In: Schwarz KP (ed) Geodesy Beyond 2000, The Challenges of the First Decade, Springer, Berlin Heidelberg, International Association of Geodesy Symposia, vol 121, pp 22–25, doi:10.1007/978-3-642-59742-8_4.

Wübbena G, Schmitz M, Warneke A (2019) Geo++ absolute GNSS antenna calibration. In: IGS Analysis Center Workshop 2019, 15-17 April 2019, Potsdam, Germany, URL https://s3-ap-southeast-2.amazonaws.com/igs-acc-web/igs-acc-website/workshop2019/gpp_-cal125_igs19_f.pdf